

Compliant low profile multi-axis force sensors

Oluwaseun A. Araromi, Sam Castellanos, Conor J. Walsh, Robert J. Wood

John A. Paulson School of Engineering and Applied Sciences, Wyss Institute for Biologically Inspired Engineering,
Harvard University, Cambridge, MA, USA

Abstract—The development of soft, compliant force sensors is greatly sought after in areas such as soft robotics and prosthetics. Nevertheless, solutions for measuring forces in multiple axes, while being mechanically compliant, have been few and far between. Here we present a compliant sensor able to detect forces tangential and normal to the sensor surface. The transduction mechanism is based on the deformation of laser-machined carbon fiber composite (CFC) micro-scale meanders, encapsulated within elastomers layers. Strains in the elastomer are transmitted to the meanders, causing changes in the electrical resistance of the sensor contact mechanics. Configuring the meanders in a radial pattern, segmenting them into quadrants (two antagonist pairs) and biasing the center of the sensor out-of-plane enables detection of forces in multiple axis via differential measurement. Sensors were manufactured using a custom fabrication process and exhibited high mechanical compliance with a very low form factor. The sensors were experimentally characterized and demonstrated large differential changes in resistance (up to 26 k Ω for tangential forces applied to the sensor surface). We integrated our sensor onto a soft robotic gripper finger and demonstrated the ability to detect changes in friction at the actuator surface, thus demonstrating their potential for real world applications.

Index Terms—Soft Material Robotics; Wearable Robots.

I. INTRODUCTION

Soft, compliant force sensors are greatly sought after in the realms of wearable electronics [1], wearable robotics [2], soft robotics [3], dexterous grippers [4] and prosthetics [5]. Moreover, mechanical robustness and resilience are also desired in order to increase device longevity, especially in applications where the sensor is likely to be subjected to a large degree of bending (e.g. wearable applications). Several soft or compliant sensor concepts have been proposed in the literature for measuring linear strains (e.g. for joint angle measurement) [6], [7], [8], and those optimized to measure normal pressure [9], [10], [11]. However, relatively few approaches have been developed for measuring forces in multiple degrees of freedom (DOFs).

Measurements of forces tangential to a surface (i.e. shear) can be useful for establishing the relative motion between a wearable device or a robotic prosthetic and the skin of a user, and could help to determine pressure points or areas of excessive friction. Vogt et al. developed a soft, multi-axis force sensor concept based on the deformation of micro channels in an elastomer composite filled with liquid metal [12]. Though very effective, the sensor had a thickness of several millimeters, making it less ideal for wearable applications. The compliant shear sensor design presented by Toyama et al. based on the relative translation of two

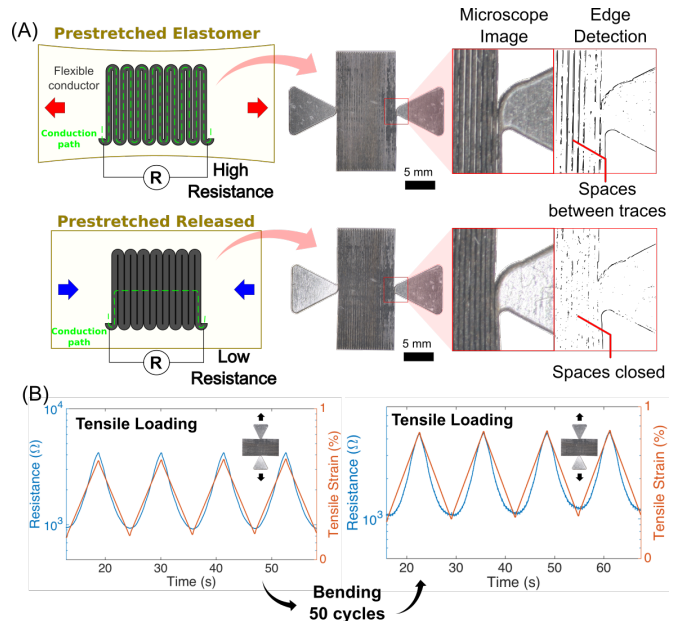


Fig. 1. Sensor working principle: (A) Flexible conductors in the shape of a meander are adhered onto a prestretched elastomer substrate. Stretching of the elastomer film changes the electrical conduction path and also the contact area between meander traces (via contact pressure). This changes the overall electrical resistance at the terminal points. (B) Example of response of transducer to tensile strain cycles. Qualitative behavior continues even after being subjected to 50 bending cycles.

planar electrodes separated by ionic liquid and has a low form factor [5]. However, the use of a liquid may result in large changes in volume or conductivity with temperature, and may present problems regarding mechanical resilience and long survivability.

Here, we present a compliant, multi-axis force sensor based on the deformation of laser-machined carbon fiber composite (CFC) micro-structures encapsulated within prestretched elastomers. The sensor working principle is outlined in Figure 1(A). The CFC, which is electrically conductive, is machined into the shape of a meander and bonded to a prestretched elastomer. In this state, the electrical conduction path is longest and the sensor exhibits a high electrical resistance. When the prestretch in the elastomer is released, the underlying elastomer compresses the meanders in-plane, causing the strands to come into contact, short-circuiting the conduction path and substantially reducing the sensor resistance. The result is a transduction mechanism with good linearity and a extremely large resistance changes (see

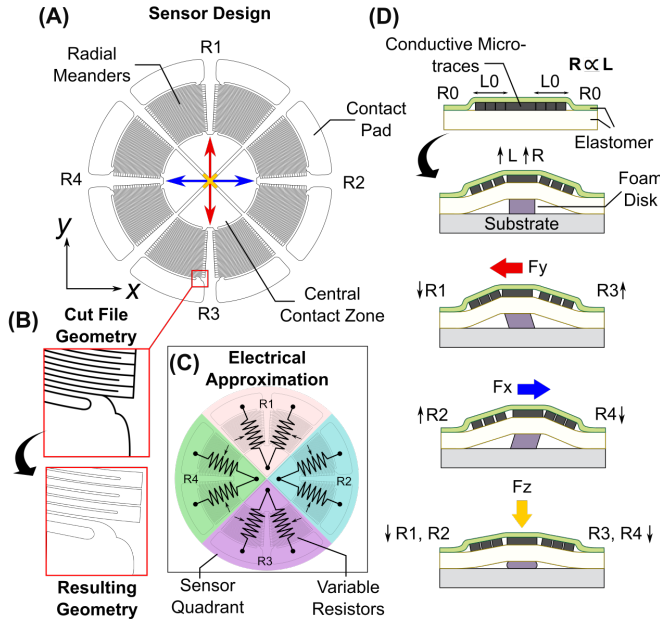


Fig. 2. Sensor design. (A) Transducer geometry. (B) Close-up of laser cut file geometry and schematic of resulting transducer geometry. (C) Transducer electrical approximation. (D) Schematic representation of the change in electrical resistance of the sensor in response to various loading conditions.

Figure 1(B). By configuring the sensor design radially and providing a mechanical bias out of plane, sensing of forces in multiple axes can be performed (Figure 2).

In section II the sensor design is discussed in detail, followed by a description the custom fabrication methodology developed to manufacture the sensor in section III. The results of an experimental characterization of the sensor is provided in section IV followed by a discussion in section V. Finally, the conclusions of our work are given in section VI.

II. SENSOR DESIGN

The fundamental sensor transduction principle is depicted in Figure 1. Prestretching elastomer films generate compressive stresses in the material. If a stiff but flexible material is bonded on top of the elastomer, the elastomer material will buckle out-of-plane when the prestretched is released, and eventually reach an equilibrium state - dependent upon the stored mechanical energy from prestretching, and the energy required to cause bending in the flexible material. However, if the flexible material is micro-structured such that it has a meander shape (as shown in Figure 1), and the space between traces is sufficiently small, releasing the prestretch will cause the meanders to buckle in-plane before bending out-of-plane. If the flexible material is conductive, the conduction path through the structure will be different between the prestretched and equilibrium states - being high in the prestretched state and low in the equilibrium state. Furthermore, the amount of prestretch governs the contact area between touching traces, mediating the resistance between each trace like a deformation-dependent variable resistor. Hence, deforming the elastomer between the equilibrium and

the prestretched states causes a change in resistance which is continuous (Figure 1(B)). Several parameters govern the value of resistance between the two states, the most pertinent are listed below:

- *Elastomer mechanical properties*: The stiffness of the elastomer film - a function of the elastic modulus and the film geometry - governs the amount of compressive stresses generated in the film for a given prestretch.
- *Elastomer prestretch*: For a given elastomer film geometry, prestretch governs the amount of compressive stresses generated in the film. Prestretch also has an impact on the linearity of the sensor, depending on if the prestretch exceeds the linear elastic range of the elastomer.
- *Meander geometry*: Governs how easily the meanders can be made to come in contact with each other (i.e. how easily the can be bent in-plane) via the spacing distance, and also sets the limits on the maximum and minimum electrical resistance. This also plays a large role in determining the mechanical compliance of the sensor.
- *Flexible conductor electrical properties*: Sets the limits on the maximum and minimum electrical resistance, for a given meander geometry.
- *Flexible conductor mechanical properties*: Dictates the ease with which the meander traces can be made to touch each other, for a given meander geometry and elastomer stiffness. This also plays a large role in determining the mechanical compliance of the sensor and the mechanical resilience.

We exploit this fundamental transduction principle to develop a sensor capable of sensing forces in multiple axes. The chosen sensor design is shown in Figure 2 and has meanders which are orientated radially, rather than linearly. The sensor design has four quadrants (two antagonistic pairs) (Figure 2(A)), which electrically can be thought of as four independent variable resistors (Figure 2(C)), where the resistance is based on the change of stretch in each quadrant, as explained above. With the aid of a soft mechanical biasing element, the sensor is displaced out-of-plane, which induces a prestretch in the sensor quadrants and offsets the central contact zone from the rest of the device.

Shear forces (forces applied tangentially to the central region of the sensor) are detected as a change in length of one resistor quadrant relative to the opposing quadrant (Figure 2(D)). For the application of normal pressure, all four sensor quadrants experience a decrease in length, and therefore a decrease in thickness.

In this work we use carbon fiber composites (CFC) to fabricate the conductive meanders for its combination of good electrical conductivity (electrical sheet resistance measured to be approximately $8 \Omega/\text{sq.}$) and mechanical flexibility, enabling the device to be able to withstand bending. Furthermore, the electrical resistance does not change substantially with applied load (for the low loads used in this work) due

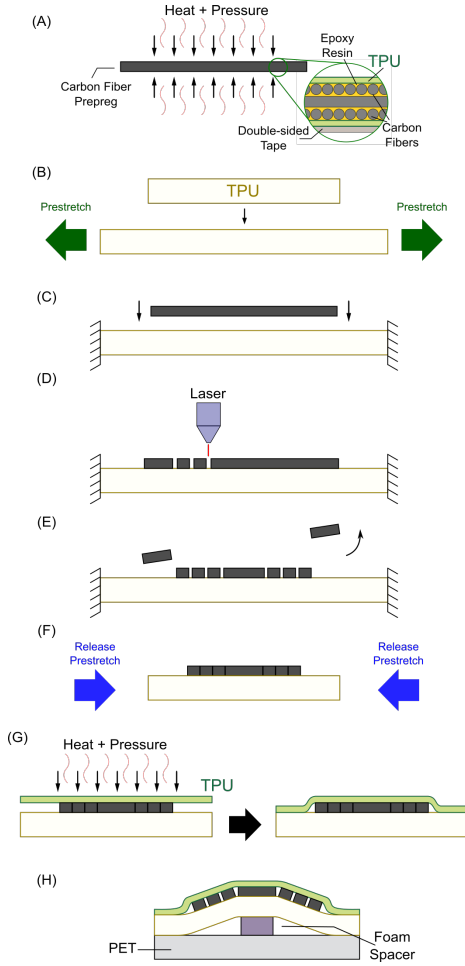


Fig. 3. Sensor fabrication procedure: (A) Carbon fiber composite (CFC) lay-up manufacture. (B) A 300 μm thick TPU film is prestretched biaxially in-plane. (C) The CFC film is adhered to the TPU using double-sided tape. (D) The CFC lay-up is micro-machined using a laser. (E) Excess CFC material removed by peeling. (F) The prestretch in the TPU is relaxed, causing the meanders of the micro-structured CFC to come into contact with each other (short circuiting the electrical conduction path). (G) The CFC meanders are encapsulated by a 30 μm TPU film by heat bonding. (H) A biasing spacer is placed underneath the encapsulated traces and the sensor bonded to a PET substrate.

to its high stiffness. Thermoplastic polyurethane (TPU) is used for the encapsulating material due to its convenience in fabrication, being able to be heat sealed to other TPU layers within seconds, facilitating rapid fabrication. We use foam as the biasing element, which enables the sensor to be sheared more easily, while allowing for a high degree of mechanical compliance. A biasing structure made from a less compliant material, such as PDMS (polydimethylsiloxane), can also be used. However, this would make the sensor stiffer and reduce sensor sensitivity.

III. SENSOR FABRICATION

A custom fabrication methodology was developed in order to fabricate our multi-axis force sensors. The methodology enables the reliable and repeatable fabrication of sensors.

First, the CFC lay-up is made by stacking three layers of carbon fiber sheets pre-impregnated with an epoxy resin (Toho Tenax, by Teijin), and sandwiching with two layers of 30 μm thick TPU. The three CFC layers are laid orthogonal to each other, as depicted in Figure 3(A). This orthogonal stacking helps to maintain the flatness of the composite by minimizing thermally induced buckling. The carbon fiber composite lay-up is then placed in a heat press and is cured using the manufacturer's recommended pressure and heat profiles.

Following the CFC fabrication, a 300 μm thick TPU film is stretched approximately 20 % biaxially in-plane using a purpose built prestretcher mechanism (Figure 3(B), see also Figure 4(A)). The CFC lay-up is cut to the desired size, backed on one side with a 5 μm thin double-sided adhesive (82600, by 3M), and adhered to the surface of the prestretched TPU. The sensor geometry is laser-machined into the CFC layup using a diode-pumped solid-state laser (by Oxford Lasers) (Figure 3(C)). The spaces between the meander traces are represented by a single cut line in the cut file geometry (see Figure 2(B)). This minimizes the spacing between the meander traces, hence reducing the amount prestretch required to make the traces come into contact with each other. This also means that the minimum distance between meander traces is determined by the laser beam width. After the laser-machining process is complete, the excess material is removed from TPU film.

The prestretch in the TPU film is released by carefully removing it from the prestretch mechanism (Figure 3(F)), and a second 30 μm thin TPU film is placed on top of the CFC and heat-pressed onto the lay-up and underlying TPU film (Figure 3(G)). This serves to encapsulate the CFC traces, fixing the traces in place and protecting them from external disturbances. This also ensures that there is no slip between the TPU layer and the CFC traces. Slip between the TPU and traces would result in a loss of in-plane compressive stress and reduce the sensor repeatability over time.

A foam disk approximately 2 mm thick is placed under the sensor at its center, and the perimeter of the sensor bonded to a PET substrate using a double-sided adhesive (Figure 3(H)). The foam disk is compressed when the transducer is bonded to the PET substrate, reducing the thickness. The foam thickness was selected as the result of a pre-characterization of different foam thicknesses, and was shown to provide good biasing while not excessively increasing the sensor overall thickness.

IV. EXPERIMENTAL CHARACTERIZATION

A. Multi-axis characterization

Figure 4 shows the various steps of the fabrication process used to manufacture the sensors used in the experimental characterization. The total sensor diameter is 20 mm (Figure 4), the excess TPU surrounding the sensor is left in place to help with device handling and electrical connections. The sensor demonstrates a high degree of mechanical compliance

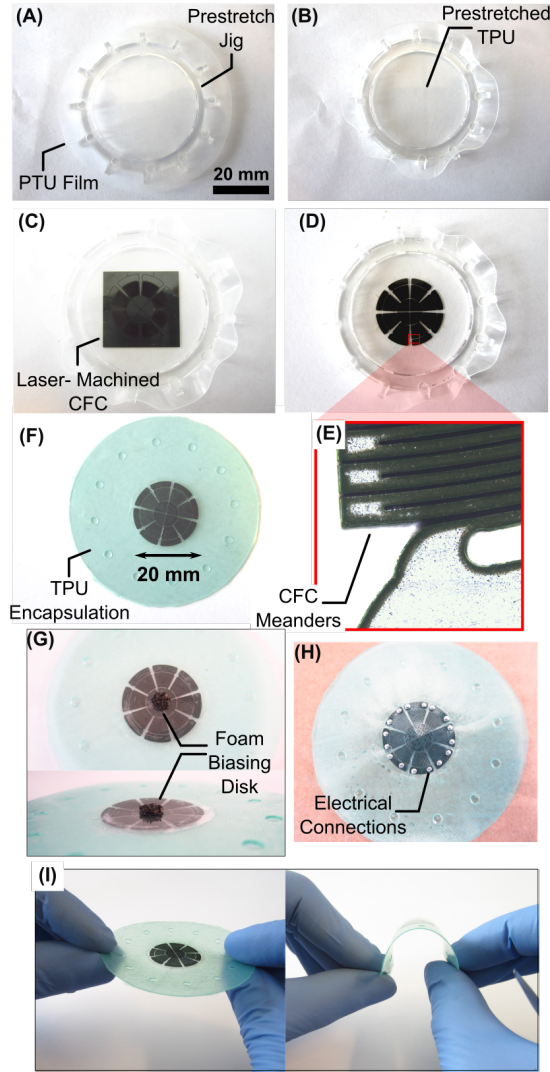


Fig. 4. Fabricated force sensor: (A) The TPU film and prestretching mechanism placed underneath (made from transparent plexiglass). (B) The stretched TPU film. (C) Laser-machined CFC adhered to the stretched TPU. (D) Excess CFC material removed post laser machining. (E) Microscope of meander geometry (shaded in green for clarity). (F) Encapsulated sensor device. (G) Foam disk adhered to the sensor underside. (H) Electrical connection made using metal pins inserted through CFC and TPU layers. (I) Demonstration of sensor compliance and low form factor.

and conformability. The thickness of the meanders is approximately 70 μm and spaces between meanders approximately 30 μm . We characterize our sensor using the experimental set-up schematically depicted in Figure 5. A probe made of plexiglass is attached to the center of the sensor at one end, and to the moving head of an Instron mechanical tester (model 5544A) at the other. For ease of characterization, electrical connections are facilitated via metal pins which puncture through the sensor contact pads (Figure 4), making a through-hole connection. The resistance of the each of the sensor quadrants is measured using a four-point measurement technique in order to mitigate the effect of contact resistance.

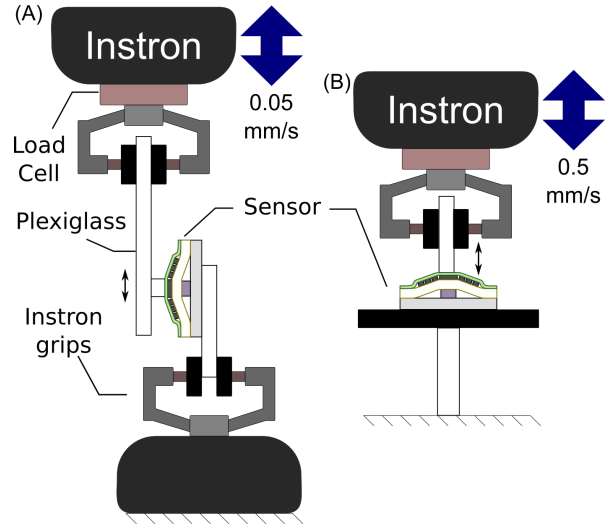


Fig. 5. Schematic of experimental characterization set-up. (A) Test configuration for characterizing forces in x and y . (B) Test configuration for measuring normal forces.

Data acquisition was performed using a National Instruments DAQ board and synchronized with the mechanical data via the Instron software interface (sample rate was 10 ms). Forces were applied tangentially to the sensor surface in both in-plane dimensions with a magnitude of ± 1 N at a speed of 0.05 mm/s for three cycles. A normal force was also applied to the sensor in the range -8 N and 0 N at a speed of 0.5 mm/s for three cycles (the force and speed settings were increased for the normal force tests due to the increased range of motion in the sensor in the normal direction).

Figure 6 shows the results of the sensor characterization. The results are presented as the difference in the resistance of antagonist sensor quadrants, and subtracted by the initial differential value i.e. $R_x = (R_1 - R_3) - (R_1^0 - R_3^0)$ and $R_y = (R_2 - R_4) - (R_2^0 - R_4^0)$, where subscript numbers 1, 2, 3 and 4 correspond to the four sensor quadrants, the superscript 0 denotes the value at time = 0 i.e. at the start of the experiment, and R_x is the and R_y are the differential resistances plotted in Figure 6. As can be seen from the figure, a substantial differential resistance was measured for the shear measurements. A differential resistance $R_x > 25$ k Ω was seen for shear in the x -direction over the applied force range (Figure 6(A)). This is approximately 10 times greater than the variation seen in the orthogonal antagonist quadrant pair R_y . Moreover, both the sensor linearity (R^2 value of 0.9829) of and repeatability over the three cycles are acceptable for many robotic sensing applications (see section IV-B).

A lower differential resistance R_y can be seen for shear in the y -direction (approximately 6 k Ω) as seen in (Figure 6(B)), we attribute this to manufacturing error and the difficulty in placing the plexiglass probe perfectly in the center of the device. Despite this, the linearity in the sensor signal remains (R^2 value of 0.9629). The response of the sensor to normal

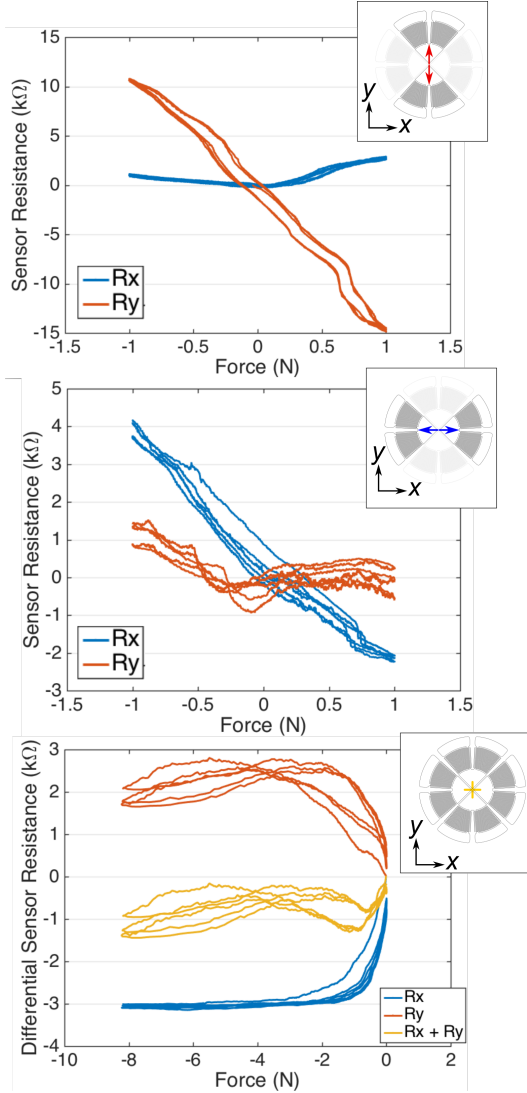


Fig. 6. Results of sensor experimental characterization: (A) Results for applied forces in x -dimension. (B) Results for applied forces in y -dimension. (C) Results for applied forces in z -dimension.

pressure is shown in Figure 6(C). The differential resistances R_x and R_y approximately mirror each other about the zero value. At lower values of compressive force, below 2 N, there is a relatively steep change in the differential resistances (between 2 - 3 N). For compressive forces greater than 2 N, the differential resistances saturate. This can be explained through the compression of the foam core, which ceases to act as a biasing mechanism for the sensor, and thus the associated prestretch in the device is released.

B. Sensor integration with a soft actuator

We integrate our sensor technology onto the finger actuator of the soft robotic gripper developed Galloway et al. [4] in order to demonstrate the ability to detect contact forces in real-world robotic systems. Sensor integration was performed by heat-pressing a sensor onto a TPU coated textile, and

threading the textile onto purpose made holes cast into the soft actuator structure. The result of the sensor integration is shown in Figure 7 (the TPU material surrounding the sensor was kept in place as it proved convenient for making electrical connections). A circular PDMS film was attached to the central contact zone of the sensor to increase friction. A 1 inch diameter plastic pipe was attached to an Instron mechanical tester and was placed in the path of the actuator, and the actuator subsequently pressurized to 20 psi, causing it to curl around the pipe (Figure 7(B)). The plastic pipe was then displaced vertically at a rate of 1 mm/s until a point at which it lost contact with the surface of the actuator (occurring at approximately 16 seconds). The sensor resistance was measured simultaneously using the set-up mentioned above in section IV-A. The results of this experiment are shown in Figure 7(C). A clear difference can be seen between the differential resistance values, R_x and R_y . R_y represents the output from the antagonistic quadrant pair parallel to the direction of travel of the plastic pipe (note, R_z is not shown as this requires the development of decoupling relationship, which is beyond the scope of this preliminary investigation). The value of R_y increases gradually until it begins to plateau at around 11 seconds (indicated by the plateau in the Instron force reading). This period represents a phase where the sensor is deformed through contact with the moving pipe until it reaches a stable position and starts to slip. At 16 seconds the pipe slips completely from the grasp of the soft actuator (as indicated by the reduction in force measured by the Instron load cell), at which point the value for R_y returns to near the baseline value. The value R_x is relatively more noisy, potentially due to excessive deformation of the sensor connections as the actuator is deformed by the pipe.

V. DISCUSSION

The sensor developed in this work was fabricated using a custom manufacturing methodology and exhibits a high degree of mechanical compliance. The fabricated sensor has demonstrated the ability to detect forces applied tangentially and normally to the sensor surface. Moreover the sensor signal is reasonably linear and repeatable. The changes in electrical resistance induced by forces are in the thousands of Ohms, and hence can be measured without the use of complex signal conditioning or amplification circuits. The high compliance of the sensor enables it to conform to non-planar surfaces, such as the surface of a soft robotic gripper finger. Future work would involve the development of a model which would enable full decoupling of forces applied in all three axes (this was outside the scope of this initial study). Moreover, such a model would also prove useful for optimizing the sensor fabrication parameters, such as prestretch value and meander geometry, in order to maximize signal to noise. The effects of scaling would also be investigated in future studies, in particular, the limits of miniaturization, as this impacts the maximum spatial resolution achievable.

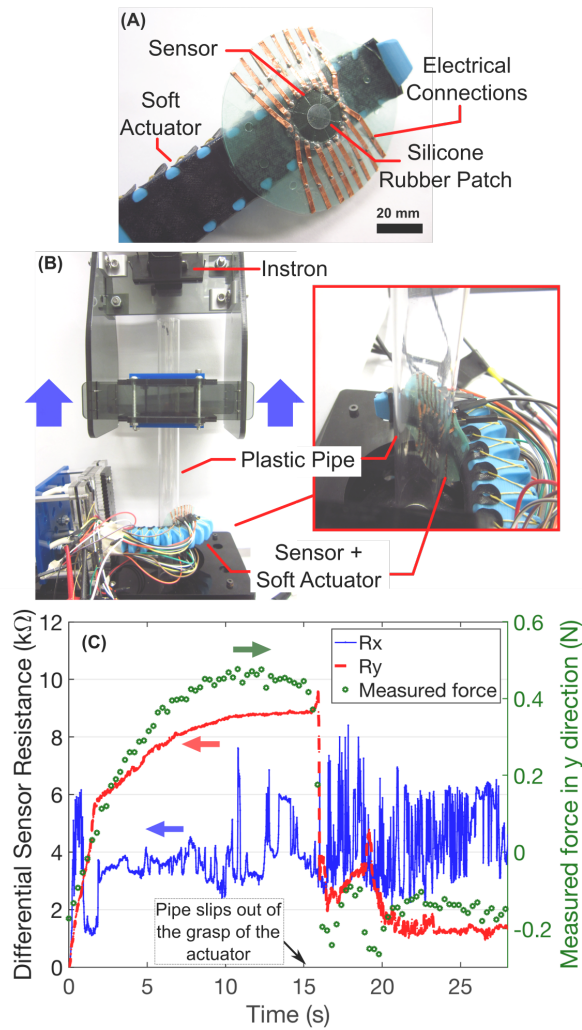


Fig. 7. (A) Integration of compliant sensor onto a soft actuator finger from a soft robotic gripper. (B) Experimental set-up for friction detection demonstration. (C) Results of friction detection demonstration.

VI. CONCLUSION

A compliant multi-axis force sensor has been described in this work. The transduction mechanism is based on changes in contact resistance between the traces of CFC meanders bonded to prestretched TPU. The sensor resistance is mediated by compressive stresses in the TPU. In order to measure forces in multiple axes, the CFC meanders are oriented radially and segmented into four quadrants (two antagonist pairs), and the central region of the sensor is offset out-of-plane by a foam biasing element. Prototype sensors were fabricated using a custom fabrication system and exhibited a high degree of mechanical compliance. The sensors demonstrated the ability to detect and distinguish forces tangential to the sensor surface, as well as normal to the sensor surface. Moreover, resistance changes in the thousands of Ohms were measured for applied tangential forces in the range ± 1 N, more than 10 times that recorded

for the orthogonal antagonist pair, and in a range which can be easily measured with simple electronic circuits. The sensor was integrated onto the surface of a soft robotic gripper finger and friction force detection was demonstrated, validating the efficacy of our technology in real world systems.

ACKNOWLEDGMENT

This material is based upon the work supported by the Defense Advanced Research Projects Agency (DARPA), Warrior Web Program (Contract No. W911NF-14-C-0051). This work was also partially funded by the Wyss Institute for Biologically Inspired Engineering and the John A. Paulson School of Engineering and Applied Sciences at Harvard University. The authors would like to gratefully acknowledge Kaitlyn Becker for her assistance with the soft robotic gripper demonstration, and Neel Doshi his assistance with carbon fiber composite characterization. The prototypes presented were enabled by equipment supported by the ARO DURIP program (award #W911NF-13-1-0311)

REFERENCES

- [1] D. H. Kim and J. a. Rogers, "Stretchable electronics: Materials strategies and devices," *Advanced Materials*, vol. 20, no. 24, pp. 4887–4892, 2008.
- [2] F. Panizzolo, I. Galiana, A. T. Asbeck, C. Sivi, K. Schmidt, K. G. Holt, and C. J. Walsh, "A biologically-inspired multi-joint soft exosuit that can reduce the energy cost of loaded walking," *Journal of Neuroengineering and Rehabilitation*, vol. submitted, no. 1, p. 43, 2016.
- [3] R. F. Shepherd, F. Ilievski, W. Choi, S. A. Morin, A. A. Stokes, A. D. Mazzeo, X. Chen, M. Wang, and G. M. Whitesides, "Multigait soft robot," *Proceedings of the National Academy of Sciences*, vol. 108, no. 51, pp. 20 400–20 403, dec 2011.
- [4] K. C. Galloway, K. P. Becker, B. Phillips, J. Kirby, S. Licht, D. Tchernov, R. J. Wood, and D. F. Gruber, "Soft Robotic Grippers for Biological Sampling on Deep Reefs," *Soft Robotics*, vol. 3, no. 1, pp. 23–33, mar 2016.
- [5] S. Toyama, Y. Tanaka, S. Shirogane, T. Nakamura, T. Umino, R. Uehara, T. Okamoto, and H. Igarashi, "Development of Wearable Sheet-Type Shear Force Sensor and Measurement System that is Insusceptible to Temperature and Pressure," *Sensors*, vol. 17, no. 8, p. 1752, 2017.
- [6] A. Atalay, V. Sanchez, O. Atalay, D. M. Vogt, F. Haufe, R. J. Wood, and C. J. Walsh, "Batch Fabrication of Customizable Silicone-Textile Composite Capacitive Strain Sensors for Human Motion Tracking," *Advanced Materials Technologies*, vol. 1700136, p. 1700136, 2017.
- [7] A. P. Gerratt, H. O. Michaud, and S. P. Lacour, "Elastomeric Electronic Skin for Prosthetic Tactile Sensation," *Advanced Functional Materials*, vol. 25, no. 15, pp. 2287–2295, 2015.
- [8] Y. Menguc, Y.-L. Park, H. Pei, D. Vogt, P. M. Aubin, E. Winchell, L. Fluke, L. Stirling, R. J. Wood, and C. J. Walsh, "Wearable soft sensing suit for human gait measurement," *The International Journal of Robotics Research*, vol. 33, no. 14, pp. 1748–1764, 2014.
- [9] D. P. J. Cotton, I. M. Graz, and S. P. Lacour, "A multifunctional capacitive sensor for stretchable electronic skins," *IEEE Sensors Journal*, vol. 9, no. 12, pp. 2008–2009, 2009.
- [10] B. Nie, R. Li, J. Cao, J. D. Brandt, and T. Pan, "Flexible Transparent Iontronic Film for Interfacial Capacitive Pressure Sensing," *Advanced Materials*, pp. n/a–n/a, 2015.
- [11] J.-Y. Sun, C. Keplinger, G. M. Whitesides, and Z. Suo, "Ionic Skin," *Advanced Materials*, vol. 26, no. 45, pp. 7608–7614, 2014.
- [12] D. M. Vogt, Y.-L. Park, and R. J. Wood, "Design and Characterization of a Soft Multi-Axis Force Sensor Using Embedded Microfluidic Channels," *IEEE Sensors Journal*, vol. 13, no. 10, pp. 4056–4064, oct 2013.